Engineering Science and Technology, an International Journal 19 (2016) 956–963

HOSTED BY

Contents lists available at ScienceDirect

Engineering Science and Technology, an International Journal

journal homepage: http://www.elsevier.com/locate/jestch

Full Length Article

Friction and wear behavior of nitrogen-doped ZnO thin films deposited *via* MOCVD under dry contact

U.S. Mbamara [a], B. Olofinjana [b,c,*], O.O. Ajayi [c], C. Lorenzo-Martin [c], E.I. Obiajunwa [d], E.O.B. Ajayi [b]

[a] Department of Physics, Federal University of Technology, Owerri, Nigeria
[b] Department of Physics and Engineering Physics, Obafemi Awolowo University, Ile-Ife, Nigeria
[c] Tribology Section, Argonne National Laboratory, 9700 S. Cass Avenue, Argonne, IL 60439, USA
[d] Center for Energy Research and Development, Obafemi Awolowo University, Ile-Ife, Nigeria

ARTICLE INFO

Article history:
Received 13 October 2015
Received in revised form
25 December 2015
Accepted 6 January 2016
Available online 1 February 2016

Keywords:
Thin films
Friction
Wear
Optical microscopy
Profilometry

ABSTRACT

Most researches on doped ZnO thin films are tilted toward their applications in optoelectronics and semiconductor devices. Research on their tribological properties is still unfolding. In this work, nitrogen-doped ZnO thin films were deposited on 304 L stainless steel substrate from a combination of zinc acetate and ammonium acetate precursor by MOCVD technique. Compositional and structural studies of the films were done using Rutherford Backscattering Spectroscopy (RBS) and X-ray Diffraction (XRD). The frictional behavior of the thin film coatings was evaluated using a ball-on-flat configuration in reciprocating sliding under dry contact condition. After friction test, the flat and ball counter-face surfaces were examined to assess the wear dimension and failure mechanism. Both friction behavior and wear (in the ball counter-face) were observed to be dependent on the crystallinity and thickness of the thin film coatings.

1. Introduction

Over the years, there has been high demand for friction and wear control in all aspects of science and technology. This is because of the enormous amount of energy that is being lost in various systems. In addition, friction and wear reduction do not only bring about energy saving and efficiency, they also increase reliability and durability, which ultimately bring about customer satisfaction.

There are many approaches that have been used in reducing friction and wear. The application of lubricants between moving surfaces to partially or fully separate the contacting surfaces, which then allows for easier movement, is the most common approach. Since failure of engineering materials through friction, wear and fatigue often takes place on the surface of the material, modifying the material surface usually plays important role in reducing friction and wear. Techniques employed in surface modification include, but not limited to, carburization [1,2], plasma nitriding [3,4], ion implantation [5,6], surface texturing [7,8], laser surface modification [9] and thin film coatings [10–12].

Varieties of thin film coatings exist, and there is normally a suitable coating for a given engineering application. In tribological application, the coatings need to posses low shear strength so as to carry the pressure generated between opposing surfaces, thus allowing easier sliding. A large variety of coatings that meet this restriction have been developed, and these can be grouped as soft metal coatings, transition metal dichalcogenide coatings, carbon-based coatings, oxide coatings, sulfate coatings, and polymer coatings, among others.

Until recently, most researches on doped ZnO thin films were more about their applications in UV-light emitters, transparent high power electronics, surface acoustic wave devices, piezoelectric transducers and so on. However, research on the tribological properties of doped ZnO is still evolving. The open structure and favorable coordination number of ZnO could allow for accommodation of external atoms as zinc or oxygen substitutes. This permits the formation of defects through doping, which can cause the formation of slip systems that can alter the electronic structure and lower the shear strength. Thin film coatings of alumina doped ZnO have been shown to have low friction coefficient and better wear performance than pure ZnO thin film coatings [13]. Furthermore, compositing ZnO with organic polymer such as nylon and polyimide has also been shown to improve tribological performance [14–17].

In this work, nitrogen-doped ZnO thin films were deposited on 304 L stainless steel substrate from different combinations of zinc acetate and ammonium acetate precursor using metal organic chemical vapor deposition (MOCVD) technique. Compositional and

* Corresponding author. Tel.: +234 8066762570.
E-mail address: olofinb@oauife.edu.ng (B. Olofinjana).
Peer review under responsibility of Karabuk University.

http://dx.doi.org/10.1016/j.jestch.2016.01.003
2215-0986/

Table 1
Various combinations of precursor used for the deposition of the thin films.

Coating	Precursor combination
A0	100% zinc acetate
A1	90% zinc acetate and 10% ammonium acetate
A2	80% zinc acetate and 20% ammonium acetate
A3	70% zinc acetate and 30% ammonium acetate
A4	60% zinc acetate and 40% ammonium acetate

structural studies of the films were done using Rutherford backscattering spectroscopy (RBS) and X-ray diffraction (XRD). The frictional behavior of the thin film coatings was evaluated using a ball-on-flat configuration in reciprocating sliding with the aid of a high frequency reciprocating rig (HFRR) under dry contact condition. After friction test, the flat and ball counter-face surfaces were also examined to assess the wear dimension and failure mechanism.

2. Materials and methods

2.1. Film deposition

The thin film coatings were deposited on 304 L stainless steel using the pyrolytic method of MOCVD technique. The precursor used was a combination of zinc acetate and ammonium acetate in different proportions. Five sets of coatings were produced at deposition temperature of 420 °C and gas flow rate of 2.5 dm^3/min for 2-hour deposition time using different proportions of zinc acetate and ammonium acetate. The coatings were designated as A0, A1, A2, A3 and A4 for easy identification. Table 1 shows the various combination of the precursor used. Coating A0 serves as a form of control for the other coatings since pure zinc acetate was used as the precursor.

2.2. Thin film characterization

Rutherford backscattering spectroscopy (RBS) was used to determine the stoichiometry and thickness of the thin film coatings. The RBS facility is a 1.7 MeV tandem accelerator of IBM geometry, that is, scattering configuration where the incident beam, surface normal, and detected beam are all coplanar. The incident beam was He^+ with beam current of 3.8 nA. SIMNRA software was used to analyze the spectrum that was extracted from the silicon detector of the RBS facility.

The crystal structure of the thin film coatings was determined using MD-10 mini diffractometer. A Cu-K_α radiation was used as the source of radiation. The applied voltage was 25 kV for an exposure time of 1200 seconds. Chemical phase identification was performed using a computer-based system with powder diffraction file (PDF) embedded in it. A database from the International Center for Diffraction was also used in comparing the XRD pattern of the films. The intensity data were collected over a 2θ range of 15°–50°.

2.3. Friction and wear test

Friction test was conducted with a ball-on-flat configuration in reciprocating sliding using a high frequency reciprocating rig (HFRR). Fig. 1 shows the schematic diagram of contact configuration of the HFRR used. The ball counter-face specimen was Al alloy 2017 with a diameter of 12.7 mm. The ball hardness is 1.2 GPa (66 R_B) with elastic modulus (E) of 72.4 GPa and Poisson's ratio (ν) of 0.3. Six samples of flat were tested – the uncoated substrate with isotropic finish similar to the coatings (baseline) and the substrates coated with thin films using the various precursor combinations as listed in Table 1. The surface properties of the coatings have been reported earlier [18]; however, Table 2 shows the 2-D roughness data (R_a) of the coatings.

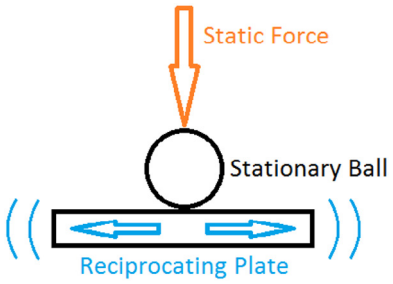

Fig. 1. Schematic diagram of reciprocating ball-on-flat contact.

For each test, flat and ball specimens were mounted on their respective holders and fixed to the test rig. The load was initiated by applying dead weight of 10 N, which imposes a nominal Hertzian contact pressure of 0.35 GPa, while the stroke length was set to 20 mm. The reciprocating speed was 60 rpm for a test time of ten minutes.

Frictional force (F) was continuously monitored for the entire duration of each test. A computer data acquisition system was used to record sliding friction force (F) at relatively high acquisition rate. The coefficient of friction (μ) defined as the ratio of the frictional force (F) to the normal force (N) was then calculated.

At the conclusion of each test, wear dimensions on ball and flat samples were measured by optical microscope and optical profilometer respectively. Worn surfaces were also examined to assess the wear mechanisms.

3. Results and discussion

3.1. Compositional study and thickness analysis

The compositional study and thickness analysis were carried out by RBS. The RBS spectrum of the control coating (A0) is shown in Fig. 2(a). The expected elements zinc and oxygen were detected, with zinc to oxygen ratio of 1:1. This ratio is consistent with elemental composition of pure crystalline ZnO. The RBS spectra of the other coatings from various combination of zinc acetate and ammonium acetate precursor were all similar. Fig. 2(b) shows a typical spectrum of the nitrogen-doped ZnO. The presence of Zn, O and N is clearly manifested. Both spectra depict two distinct sections, the substrate section and the coating section centered around 1450 keV energy. The simulated spectrum is based on hypothetical data in the database of the analyzing software for the elements envisaged. Then based on the simulated spectrum, the read data from the sample are characterized. Each element detected is matched with the database for identification, while the overall concentration of the detected elements gives rise to the thickness of the thin film.

The stoichiometry of the doped zinc oxide coatings exhibited no particular trend with respect to the proportion of zinc acetate and ammonium acetate in the precursor. Each doped zinc oxide coating gave an approximately consistent Zn:O:N ratio of 5:4:1, irrespective of the percentage of ammonium acetate (providing the nitrogen) in the prevailing precursor. Mbamara et al. (2012) [19] had

Table 2
2D roughness data (R_a) of coatings.

Coatings	Roughness R_a (nm)
A0	200.91
A1	203.95
A2	164.14
A3	145.76
A4	121.93

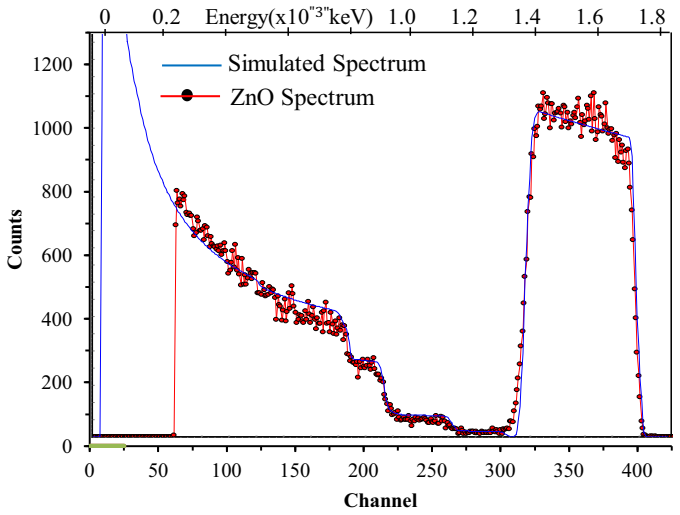

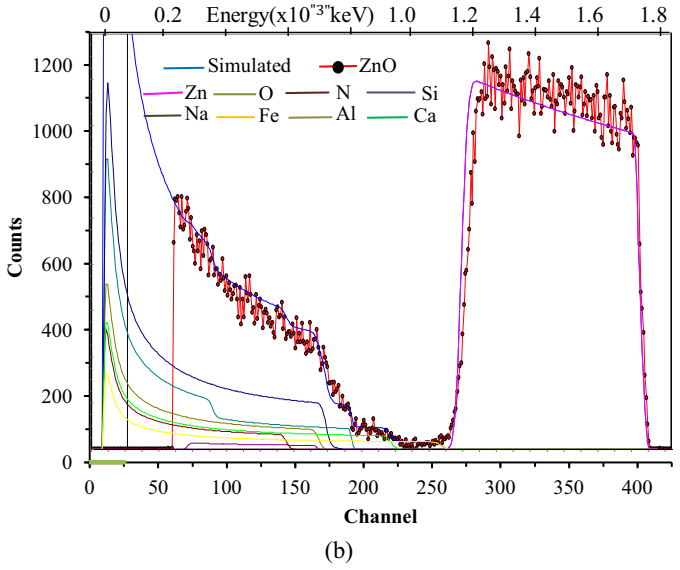

Fig. 2. RBS spectrum of (a) ZnO and (b) typical nitrogen-doped ZnO thin films.

suggested the possibility of a threshold in the ratio of zinc acetate to ammonium acetate in the precursor, beyond which the amount of nitrogen does not vary. Although this still needs further investigation, such threshold may likely be a single digit percentage or even less. Since the focus is on nitrogen as a dopant in ZnO thin film, a fraction of one percent or less of ammonium acetate is suggested for subsequent investigation.

The thickness trend as calculated from the RBS is shown in Fig. 3. Coating A4 had the lowest thickness, even lower than coating A0, which was pure ZnO. The thickness of all the coatings was, however, less than 1 μm. For the doped samples, there appeared to be a trend in the thickness, whereby the thickness was highest at lowest precursor dopant percentage and progressively decreased as the dopant percentage increased. It appears that the presence of the dopant in the precursor distinctly altered the affinity and cohesion of the deposited particles with each other. With this, it is evident that the nucleation rate in the hot zone depends on the dopant concentration in the precursor. The rate of chemical reaction in the hot chamber may have been impeded as the concentration of the precursor dopant increases. On the other hand, the MOCVD technique being more kinetic dependent than diffusion dependent [20], there

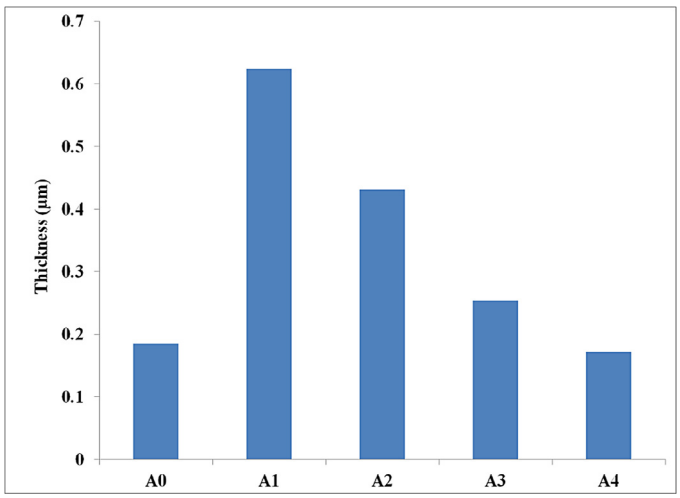

Fig. 3. Thickness of coatings obtained from RBS.

may have been an increase of kinetic reaction processes as the ratio of ammonium acetate decreases.

3.2. Crystal structure of the thin films

X-ray diffraction spectra of the coatings are presented in Fig. 4(a–e). For coating A0, peaks occurred at diffraction angles: $2\theta = 30.40°$, 32.66° and 34.72°. The peak 30.40° corresponds to (100) plane, 32.66° to (002) plane and 34.72° to (101). The presence of these peaks shows that the coating is crystalline ZnO with hexagonal structure. The dominance of the (002) line suggests a texture in which the *c* axis preferentially aligned perpendicular to the substrate.

For the doped coatings, the peaks increased steadily as the dopant component increases all through, while the structure mirrored that of hexagonal ZnO with the (100), (101) and (002) planes occurring at various diffraction angles. This reveals that the crystallinity increased as the dopant component increased. The presence of nitrogen as a dopant in ZnO had earlier been reported as being responsible for the lower crystallinity of the doped material, as compared with the undoped material [21,22]. Comparing it with the thickness, it can be seen that the crystallinity increased as the thickness decreased. Perhaps at some point during deposition process, the surface becomes saturated with crystallites, while further nucleation and radial growth cease, making the crystallite assume a columnar structure [23]. The crystallinity appears to have been controlled by the precursor mixtures, which ultimately led to different microstructure. MOCVD involves homogeneous gas phase reactions which occur in the gas phase, and heterogeneous chemical reactions that occur on or near the vicinity of a heated substrate, leading to the formation of the films. Physical and chemical properties can also be controlled by the reaction chemistry in the working chamber, and this depends on a number of factors, such as the deposition temperature, pressure, gas flow rate, reactor geometry and so on.

3.3. Frictional behavior

Friction variation with time during the test is shown in Fig. 5. The coefficient of friction for the uncoated substrate started with a value of 0.01 and quickly jumped to a value of 0.44. Thereafter, the value ranged between 0.36 and 0.46, with the highest value occurring around 523 seconds. This kind of frictional behavior is as a result of extensive material interaction exhibited by contacting

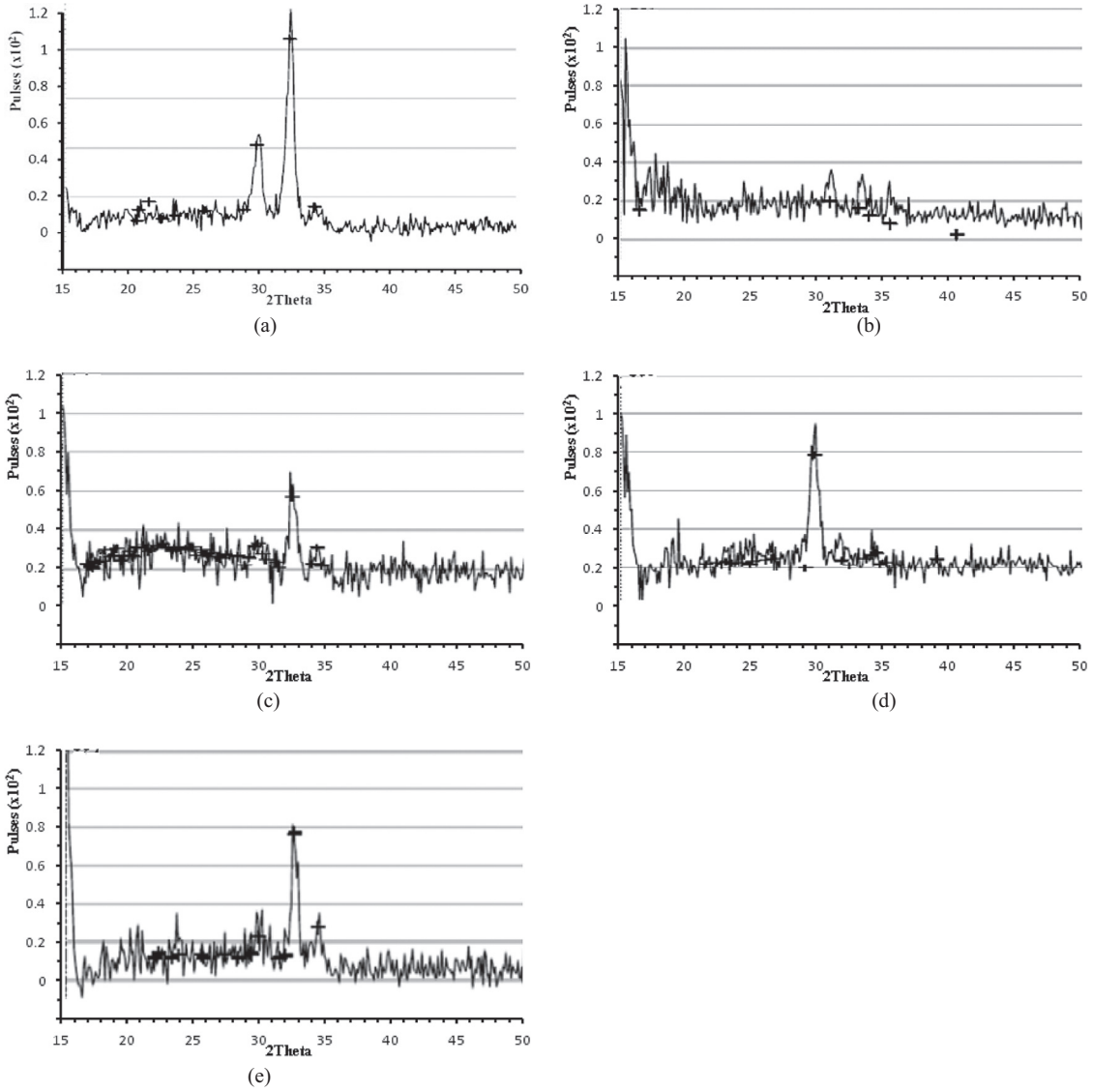

Fig. 4. XRD spectrum of coating (a) A0, (b) A1, (c) A2, (d) A3, and (e) A4.

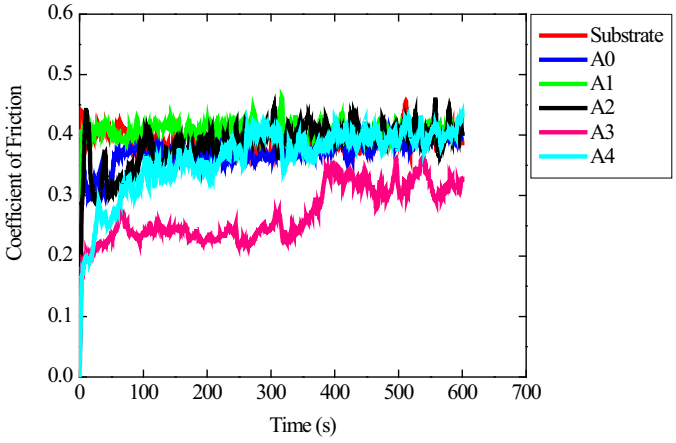

Fig. 5. Coefficient of friction as a function of time during sliding.

surfaces sliding under dry contact condition. The sliding may lead to high shear stresses and strains at the contacting surfaces, resulting in high coefficient of friction and in the extreme case intense plastic deformation [24]. Coating A0 started with a friction coefficient of 0.13 and increased rapidly to a value of 0.38. The friction coefficient then dropped to 0.29 and rose almost immediately, ranging between 0.35 and 0.41 for the remaining duration of the test. For coating A1, the coefficient of friction started with a value of 0.02 and quickly rose to a value of 0.41. The value then ranged between 0.38 and 0.47 for the rest of the test. Coating A2 started with a friction coefficient of 0.05. It then maintained values ranging between 0.28 and 0.47 during the test. The coefficient of friction for coating A3 started with a value of 0.02. It then increased to values within the range of 0.22 and 0.37. In the case of coating A4, friction coefficient started from the origin, increasing rapidly and reaching a maximum value of 0.44 at the end of the test. In all, coating A3 showed the lowest coefficient of friction value with significant reduction in the value of coefficient of friction when compared to the uncoated substrate.

Trends of frictional behavior were the same for all coatings. All the tests started out with relatively low coefficient of friction values and then transited rapidly to higher coefficient friction values. This

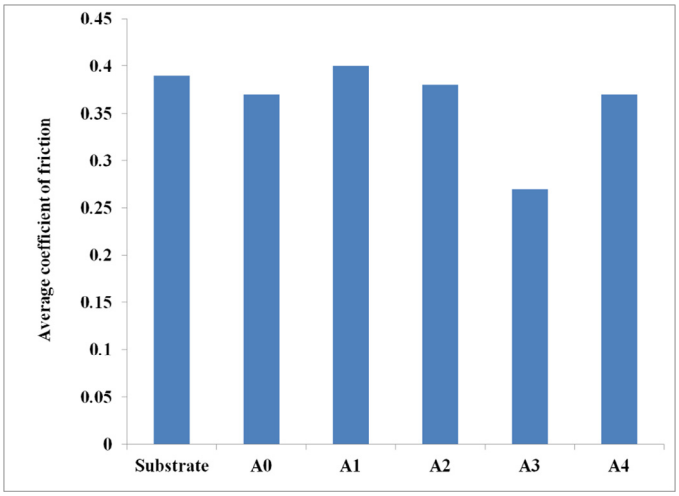

Fig. 6. Average coefficient of friction for entire duration of the test.

transition to higher friction coefficient values coincided with wearing through of the coatings. The dynamics of oxide thin film coating debris as a third body participant at contact interface comes into play. Oxides typically have high friction and they are inherently brittle forming abrasive wear debris [25–27]. After initial rubbing, the thin film breaks up and a 'clean' surface comes in contact with the ball, therby altering the bonding forces between the contacting surfaces. After this initial stage, the wear debris can be trapped in-between the sliding contact and thereby act as abrasive between the contacts [28]. This roughens the counter-face and then results in high coefficient of friction value.

Fig. 6 shows the average coefficient of friction for all the flat specimens. The average coefficient of friction covers the entire duration of the test, including run-in and steady state. Therefore it does not represent the real friction behavior of the samples. The friction transition as a function of time, which is often a reflection of change and transition in mechanism or surface damage, was not accurately reflected in the plot.

Coating A3 had the lowest value of coefficient of friction while other coatings showed higher values, with that of coating A1 even higher than that of the substrate. Although it was established that all the nitrogen-doped coatings had the same stoichiometric ratio, the difference in the friction behavior may have been due to their crystallinity and thickness. The different crystallinities resulting from different microstructures may also lead to differences in the interactions between the coatings and ball surface asperities. This will in turn result in differences in the amount of material transfer, and hence in friction and wear. Also possibly, increase in coating thickness could result in the accumulation of larger residual tensile stress, which may affect the adhesion of the thin film to the substrate.

3.4. Wear analysis

The volume of material removed (wear) from the ball counter-face was estimated using the expression [29]

$$V = \pi d^4/64r$$

where d is the wear scar diameter on the ball and r is the ball radius. The wear scar diameter was measured with the aid of optical microscope while the ball radius is 12.7 mm. Fig. 7(a) and (b) shows optical micrograph of the ball counter-face for the uncoated substrate and a typical coating.

The summary of the wear volume for the ball counter-face for all the flat samples is shown in Fig. 8. The wear behavior of the ball

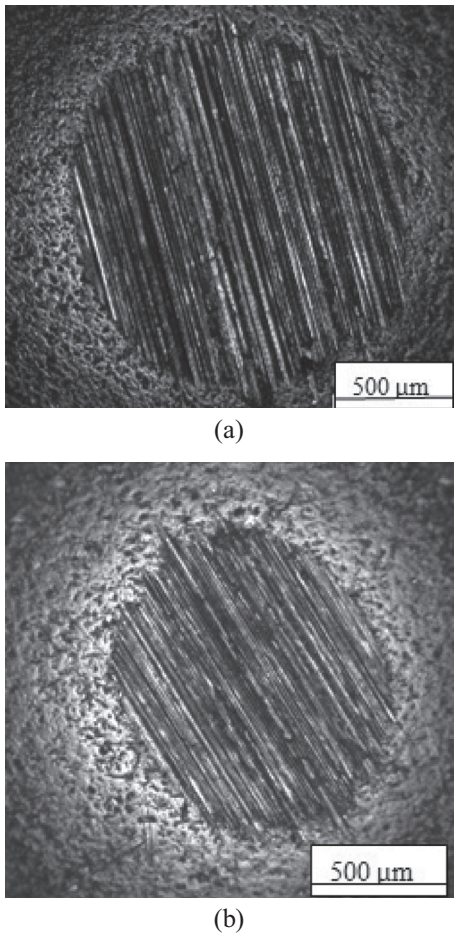

Fig. 7. Optical micrograph of ball counter-face for (a) uncoated substrate and (b) typical coating.

counter-face for the flat samples is strongly related to the friction behavior for each pair. Coating A3 had the lowest wear volume while the wear volume on the ball counter-face for other coatings was higher than that for the substrate. This is an indication that coating A3 actually protected the ball counter-face to a certain extent before damage occurred. This is expected as the average coefficient of friction for

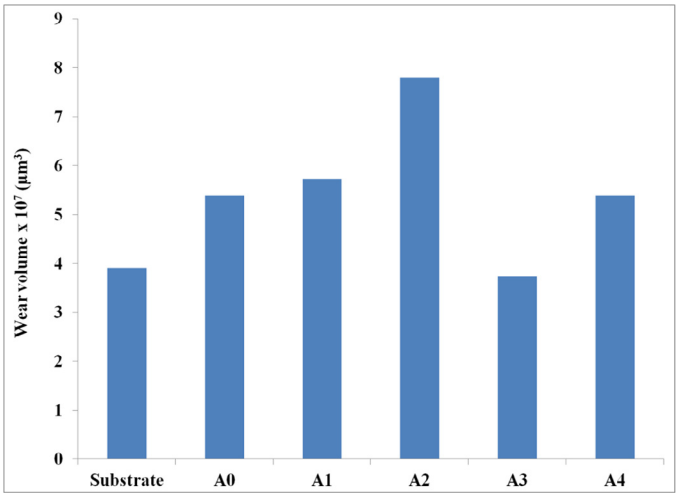

Fig. 8. Summary of ball wear volume for all flat samples.

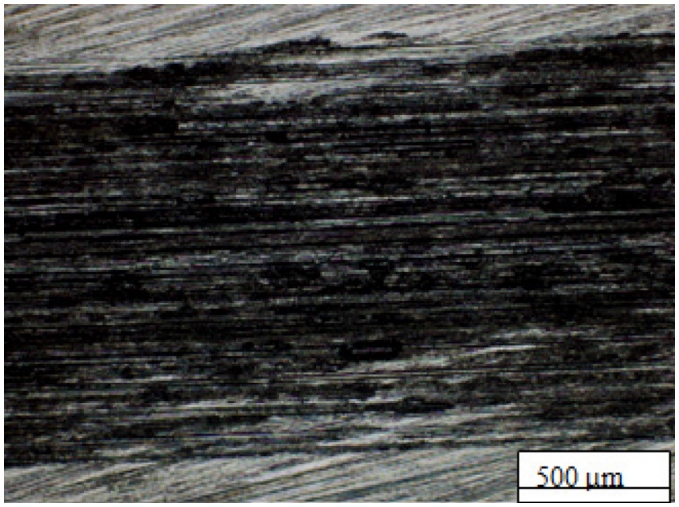

(a)

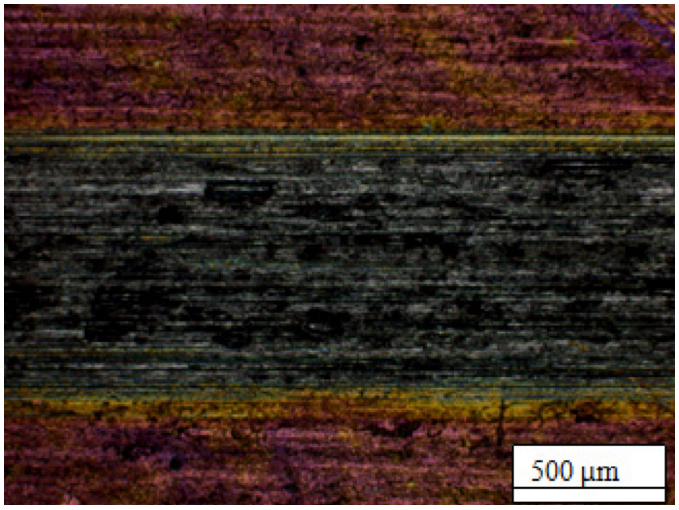

(b)

Fig. 9. Optical micrograph of (a) substrate and (b) typical coating after the friction test.

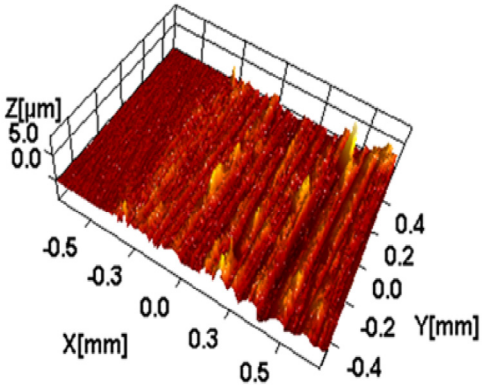

(a)

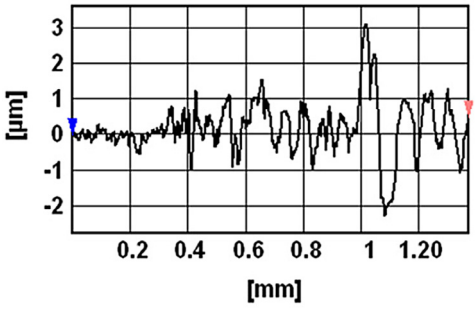

(b)

Fig. 10. (a) 3D and (b) 2D optical profile of substrate after the friction test.

coating A3 was lower than for the other coatings. This will reduce the shear stresses imposed on the coating, thereby leading to reduction in wear [28]. The other coatings possibly got damaged and worn through more quickly, leading to metal–metal contacts that resulted in higher coefficients of friction and wear. Some earlier workers have also noted that one of the shortcomings of oxide thin film coatings is that they are inherently brittle, leading to crack formation under stress, and subsequently form abrasive debris, which could then cause substantial damage on the ball counter-face [26].

As observed from the optical micrograph, the ball counter-face wear occurred predominantly by abrasive mechanism as indicated by the deep scratches in the direction of sliding. Some dark patches can also be seen in the wear tracks. This suggests that wear also occurred by formation and removal of oxide layers. However, the predominant mechanism was abrasion as the oxide formation and removal mechanism appeared to be very minimal. As the soft ball counter-face moves through the flat, deformation occurs, causing high tension and stresses in the ball surface, until they exceed the material strength, thereby resulting in material detachment (wear) through abrasive mechanism [30–32].

Fig. 9(a) and (b) shows the optical micrograph of the uncoated substrate and a typical coated flat surface after the friction test. From the micrographs, no overall material removal (wear) occurred in the flats but rather transfer of material, although it can be seen that all the coatings actually wore off probably by polishing, and in some cases mild abrasion which could have occurred at the initial stage of sliding. Different mechanisms and kinetics of material transfer from the ball counter-face, which occurred during sliding, could eventually lead to material buildup on the flats after the removal of the coatings. This may also explain why the coefficients of friction were low initially and subsequently rise to higher values typical of metal–metal interaction. The plowing action of the coating debris (which is abrasive) generated by the coating failure may have also increased the friction [28]. Subsequently, material transfer from the ball counter-face to the partially exposed stainless steel substrate occurred.

Since the wear volume is the product of the stroke length and the cross-sectional area of wear, the relative amount of material transfer onto the flat after reciprocating sliding test was determined by the cross-sectional area of wear track from the 2D profilometry. Figs. 10 and 11 show the 2D and 3D optical profile of the uncoated flat samples and a typical coating after the friction test. All the surface profiles of the flat samples clearly showed evidence of substantial material buildup which occur during sliding.

The summary of the volume of material transfer to the flats is shown in Fig. 12. The highest transfer occurred in the uncoated substrate, while among the coatings A2 had the highest material transfer on it. Consistent with the wear volume on the ball, A3 had the lowest material transfer on it. This goes to show that coating A3 to some extent protected the ball counter-face from wear. Indeed the different crystallinities resulting from the different microstructures of the coatings could have led to some differences in interactions between the coatings and the ball surface asperities.

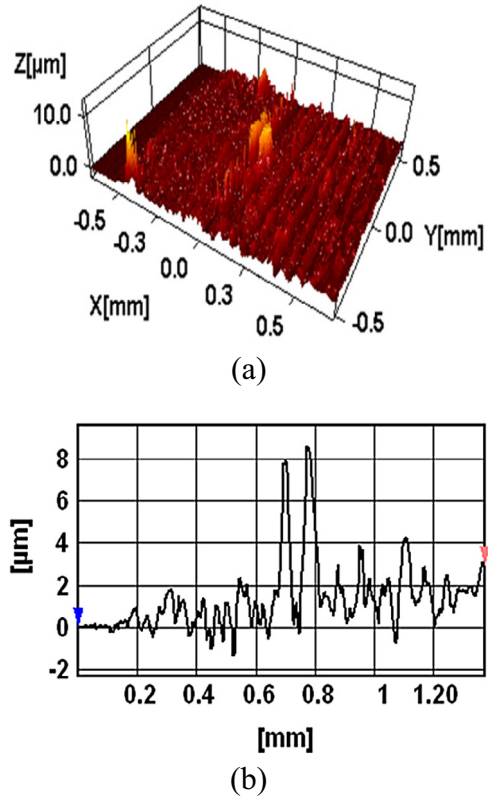

Fig. 11. (a) 3D and (b) 2D optical profile of a typical coating after the friction test.

4. Conclusion

Nitrogen-doped ZnO thin films were deposited by MOCVD technique at deposition temperature of 420 °C and gas flow rate 2.5 dm^3/min on 304 L stainless steel using different proportions of zinc acetate and ammonium acetate as precursor. RBS and XRD analyses were used for compositional study, thickness estimation and structure determination. While RBS confirmed the presence of the expected elements, the nitrogen-doped ZnO showed a consistent Zn:O:N ratio of 5:4:1 irrespective of the percentage of ammonium acetate in the precursor. Also, the coating thickness showed some dependence on the percentage of ammonium acetate in the precursor, as the thickness progressively decreased with the dopant percentage increase. The XRD tests showed that the thin films are crystalline with hexagonal structure. The crystallinity was also found to depend on the percentage of ammonium acetate in the precursor.

Reciprocating ball-on-flat friction test was conducted on uncoated 304 L stainless steel substrate (which served as the baseline) and all the coatings. The coatings exhibited different friction behavior during the test periods. With the exception of coating A3, the coatings had minimal or no effect on friction. The difference in friction behavior was attributed to the differences in microstructure as result of the difference in crystallinity and thickness exhibited by the thin films.

The wear behavior of the ball counter-face for all flat samples is strongly related to the friction behavior for each pair, with coating A3 having the lowest ball wear volume. The results suggest that sample A3 had the optimal precursor composition for obtaining good adherent film with low friction and wear qualities under the deposition parameters. In all, wear in ball counter-face occurred predominantly by abrasive mechanism. In all the flats, the coatings wore off at the initial stage of sliding, and subsequently material transfer occurred from the ball counter-face to the partially exposed stainless steel substrate.

It is envisaged that in applications involving the pair of 304 L stainless steel and Al alloy 2017, where friction and wear are concerns, nitrogen-doped ZnO coating with good stoichiometric composition, thickness and microstructure, in addition to good adhesive property, may be a viable option. Light tribological applications as in display units and electronic touch pads are also possible areas of use for the doped thin films.

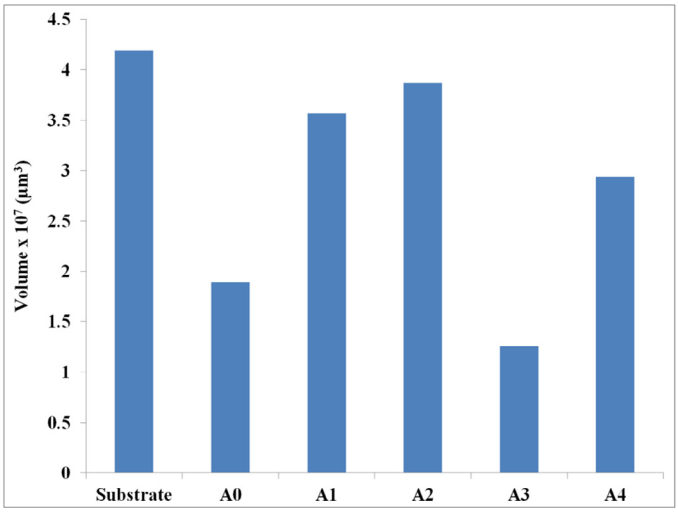

Fig. 12. Volume of material transfer for all flat samples.

Acknowledgments

The authors wish to thank the Center for Energy Research and Development, Obafemi Awolowo University, Ile-Ife, Nigeria, for the use of their RBS and XRD facility. One of the authors (BO) wishes to thank the members of the Tribology Section, Argonne National Laboratory, Argonne, USA, for their assistance in conducting the friction and wear test.

References

[1] J. Qu, P.J. Blau, B.C. Jolly, Tribological properties of stainless steel treated by colossal carbon saturation, Wear 263 (2007) 719.
[2] F.S. Chen, C.N. Chang, Effect of CH_4 addition on plasma nitrocarburizing of autenitic stainless steel, Surf. Coat. Technol. 173 (2003) 9.
[3] B. Podgornik, J. Vizintin, V. Leskovsek, Tribological properties of plasma and pulse nitrided AISI 4140 steel, Surf. Coat. Technol. 108–109 (1998) 454.
[4] Y. Xia, J. Hu, F. Zhou, Y. Lin, Y. Qiao, T. Xu, Friction and wear behavior of plasma nitrided 1Cr18Ni9Ti austenitic stainless steel under lubricated condition, Mater. Sci. Eng. A Struct. Mater. 402 (2005) 135.
[5] M.K. Lei, X.M. Zhu, Plasma based low-energy ion-implantation of austenitic stainless steel for improvement in wear and corrosion resistance, Surf. Coat. Technol. 193 (2005) 22.
[6] M. Samandi, B.A. Sheddan, D.I. Smith, Microstructure, corrosion and tribological behavior of plasma immersion ion-implanted austenitic steel, Surf. Coat. Technol. 59 (1993) 261.
[7] M. Wakuda, Y. Yamauchi, S. Kanzaki, Y. Yasuda, Effect of surface texturing on friction reduction between ceramic and steel materials under lubricated sliding contact, Wear 254 (2003) 356.
[8] X. Wang, K. Kato, K. Adachi, K. Aizawa, The effect of laser texturing of SiC surface on the critical load for the transition of water lubrication mode from hydrodynamic to mixed, Tribol. Int. 34 (2001) 703.
[9] S.H. Aldaja, O.O. Ajayi, G.R. Fenske, Z. Xu, Effect of laser surface modifications tribological performance of 1080 carbon steel, J. Tribol. 127 (2005) 596.
[10] W. Gulbinski, T. Suszko, Thin films of MoO_3-Ag_2O binary oxides – the high temperature lubricants, Wear 261 (2006) 867.
[11] T. Kubart, T. Polcar, L. Kopecky, R. Novak, D. Novakova, Temperature dependence of tribological properties of MoS_2 and $MoSe_2$ coatings, Surf. Coat. Technol. 193 (2005) 230.
[12] S.W. Zhang, State-of-the-art of polymer tribology, Tribol. Int. 31 (1998) 49.

[13] S.V. Prasad, J.J. Nainaparampil, J.S. Zabinski, Tribological behavior of alumina doped zinc oxide films grown by pulsed laser deposition, J. Vac. Sci. Technol. A 20 (2002) 1738.
[14] B. Liu, Z. Yang, J. Zhou, Tribological behavior of polyimide/zinc oxide hybrid films, Adv. Mat. Res. 105–106 (2010) 438.
[15] W. Shibo, G. Shirong, Z. Dekun, Comparison of tribological behavior of nylon composite filled with zinc oxide particles and whiskers, Wear 266 (2009) 248.
[16] H. Chakraborty, A. Sinha, N. Mukherjee, D. Ray, P.P. Chattopadhyay, A study of nanoindentation and tribological behavior of multifunctional ZnO/PMMA nanocomposite, Mater. Lett. 93 (2013) 137.
[17] B.P. Chang, H.M. Akil, R.B.M. Nasir, Comparative study of micro- and nano-ZnO reinforced UHMWPE composites under dry sliding, Wear 297 (2013) 1120.
[18] U.S. Mbamara, B. Olofinjana, C. Lorenzo-Martin, O.O. Ajayi, E.I. Obiajunwa, E.O.B. Ajayi, Surface statistical topographical properties of ZnO:N thin films deposited by MOCVD, J. Nanosci. Nanoeng. 1 (2015) 18.
[19] U.S. Mbamara, O.O. Akinwunmi, E.I. Obiajunwa, I.A.O. Ojo, E.O.B. Ajayi, Deposition and characterization of Nitrogen-doped zinc oxide thin films by MOCVD using zinc acetate-ammonium acetate precursor, J. Mod. Phys. 3 (2012) 652.
[20] B. Olofinjana, G.O. Egharevba, B.A. Taleatu, O.O. Akinwunmi, E.O.B. Ajayi, Effect of deposition temperature on some properties of MOCVD molybdenum sulphide thin films, J, Mater. Sci. Eng. B Solid State Mater. Adv. Technol. 4 (2014) 78.
[21] W. Xu, Z. Ye, T. Zhou, B. Zhao, L. Zhu, J. Huang, Low-pressure MOCVD growth of p-type ZnO thin films by using NO as the dopant source, J. Cryst. Growth 265 (2004) 133.
[22] S.T. Tan, B.J. Chen, X.W. Sun, M.B. Yu, X.H. Zhang, S.J. Chua, Realization of intrinsic p-type ZnO thin films by metal organic chemical vapor deposition, J. Electron. Mater. 34 (2005) 1172.
[23] D.M. Hausmann, R.G. Gordon, Surface morphology and crystallinity control in the atomic layer deposition (ALD) of hafnium and zirconium oxide thin films, J. Cryst. Growth 249 (2003) 251.
[24] W.M. Rainforth, A.J. Leonard, C. Perrin, A. Bedolla-Jacuinde, Y. Wang, H. Jones, et al., High resolution observations of friction-induced oxide and its interaction with worn surfaces, Tribol. Int. 35 (2002) 731.
[25] J.S. Zabinski, J. Corneille, S.V. Prasad, N.T. McDevitt, J.B. Bultman, Lubricious zinc oxide films: synthesis, characterization and tribological behavior, J. Mater. Sci. 32 (1997) 5313.
[26] H. Mohseni, T.W. Scharf, Atomic layer deposition of $ZnO/Al_2O_3/ZrO_2$ nanolaminates for improved thermal and wear resistance in carbon-carbon composites, J. Vac. Sci. Technol. A 30 (2012) 1.
[27] C. Zhimin, L. Xinchun, H. Dannong, Atomic layer deposition of zinc oxide films: effect of nanocrystalline characteristics on tribological performance, Surf. Coat. Technol. 207 (2012) 361.
[28] C. Lorenzo-Martin, O. Ajayi, A. Erdemir, G.R. Fenske, R. Wei, Effect of microstructure and thickness on the friction and wear behavior of CrN coatings, Wear 302 (2013) 963.
[29] K.L. Rutherford, I.M. Hutchings, Microscale abrasive wear testing of PVD coatings on curved substrates, Tribol. Lett. 2 (1996) 1.
[30] K. Holmberg, H. Ronkainen, A. Laukkanen, K. Wallin, Friction and wear of coated surfaces-scales, modeling and simulations of tribomechanisms, Surf. Coat. Technol. 202 (2007) 1034.
[31] A.K. Waghmare, P. Sahoo, Adhesive friction at the contact between rough surfaces using n-point asperity model, Eng. Sci. Technol. 18 (2015) 463.
[32] K.K. Alaneme, K.O. Sanusi, Microstructural characteristics, mechanical and wear behavior of aluminum matrix hybrid composites reinforced with alumina, rice husk ash and graphite, Eng. Sci. Technol. 18 (2015) 416.